CAN HIGH-RESOLUTION MARINE GEOPHYSICAL DATA BE INVERTED FOR SOIL PROPERTIES?

Mark E Vardy	Marine Geoscience, NOC, European Way, Southampton, SO14 3ZH, UK
Maarten Vanneste	Norwegian Geotechnical Institute, Oslo, Norway
Timothy J Henstock	Ocean and Earth Science, NOC, European Way, Southampton, SO14 3ZH, UK
Eugene Morgan	PSU, Department of Energy and Mineral Engineering, PA, US
Luke JW Pinson	SAND Geophysics Ltd, Southampton, SO14 6UL, UK

1 INTRODUCTION

In hydrocarbon prospection, the inversion of marine geophysical data for remote reservoir characterization has developed enormously over the past 20+ years[1]. While some techniques (e.g., waveform inversion[2]) are computationally expensive to permit widespread application across all targets, other less expensive variants (e.g., impedance[3] and amplitude-versus-angle inversion[4]) have become a standard component of most interpretation workflows. In contrast, there has been very little progress toward the remote classification of near-surface sediments through the inversion of high-resolution geophysical data[5,6,7], with both academia and industry relying on extensive coring and stratigraphic correlations.

However, accurate stratigraphic correlation can be difficult due to inaccuracies in the time-to-depth conversion of the geophysical data, and the potential for loss and/or compression of high porosity and poorly-consolidated seafloor material during the intrusive sampling process. Additionally, when dealing with near-surface sediments (top 10s m below seafloor), the sampling procedure inherently alters the nature of the sampled material, introducing uncertainties on key mechanical parameters (e.g., porosity and undrained shear strength) that are difficult to quantify.

Recently, a new inversion method was presented[8], which is based on the application of post-stack acoustic impedance inversion to high-resolution marine seismic reflection data using a genetic algorithm and a convolutional forward model. Here, we further test this approach using a synthetic example and a marine, near-surface geophysical case study from a fjordic environment in Norway. We characterize the robustness of the algorithm under a variety of noise conditions and utilize the stochastic optimization approach to derive 95% confidence limits as well as a statistically 'best' model. Furthermore, we show how, through the use of global empirical relationships, soil mechanical properties can be derived (including effective stress, over pressure, clay/sand fraction and moisture content), while, through the application of soil mechanical models (e.g., White's model), it is possible to estimate gas saturation.

In both case studies (synthetic and field), the inversion results demonstrate excellent correlation with direct sampling, even in the presence of modest noise contamination. We can identify metre-scale stratigraphic changes, as well as subtle decimetre-scale structures, such as a 40 cm thick composite landslide glide plane. The high-fidelity remote derivation of such soil properties has significant applications, both within academia and the offshore services/exploration industry.

2 INVERSION METHODOLOGY

To perform the inversion of high-resolution seismic reflection data, we use the post-stack acoustic impedance inversion algorithm of Vardy[8]. This algorithm combines a convolutional forward model[9] with a genetic optimizer[10,11] to derive an estimated acoustic impedance log at each trace location.

The algorithm works by generating an initially random family of impedance models within a user-specified impedance range, from which an associated family of synthetic traces are calculated through convolution with a theoretical source waveform (Fig. 1). The fitness of each impedance

model in the family is estimated by calculating the residual between the associated synthetic trace and the field seismic trace. The subsequent generation of models is then populated using the Stochastic Remainder technique[12], in which all models with a good fitness value are carried forward along with a random selection of those with a poorer fitness value. This new generation of models are then paired so they can be crossed-over and mutated in a randomized manner that mimics the biological process of natural selection[10], before a new family of associated synthetic traces are calculated. This process of natural selection is controlled by the user-specified cross-over and mutation probabilities, which parameterize the likelihood of two paired samples swapping (crossing-over) or a particular sample being replaced by another randomly determined value (mutating). This procedure continues until an appropriate termination clause is satisfied; either the maximum number of generations is reached, the residual between the optimum model and field trace data drops below a user-defined threshold, or the gradient of the generation-to-generation residual evolution reaches steady-state.

While a Genetic Algorithm (GA) is significantly more computationally expensive than a traditional deterministic optimization method[11], the advantages are three-fold. Firstly, the randomly generated starting generation of models means that no user-defined starting model is provided and therefore the final model is determined purely from the field seismic data. As such the final impedance model is disconnected from interpreter bias and the inversion algorithm independently derives an optimum model that statistically provides the best global fitness solution. Secondly, because a large amount of impedance space is tested during the inversion (typically 200 runs with 500 generations of 900 models for the examples presented), statistically meaningful Probability Density Functions (PDFs) can be calculated for every sample at each trace location. This allows 95% confidence limits to be calculated as well as the statistically optimum solution. Thirdly, stochastic optimization algorithms, such as a GA[10] or Simulated Annealing[13], offer a robust optimization solution even in the presence of significant noise contamination. For a GA, the mutation operator allows the algorithm to continually probe a broad region of the parameter space, affording it a mechanism to move beyond local minima in the optimization space towards the global minimum.

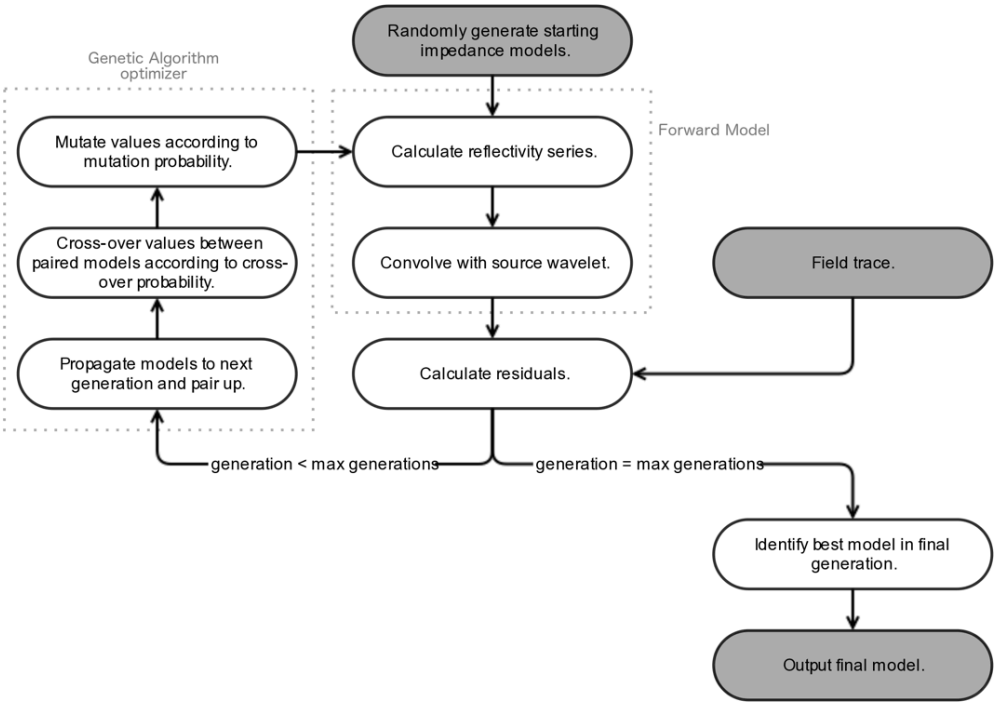

Figure 1. *Flow diagram illustrating the application of a Genetic Algorithm and convolutional model for the acoustic impedance inversion of high-resolution marine seismic reflection data. Figure adjusted from Vardy[8].*

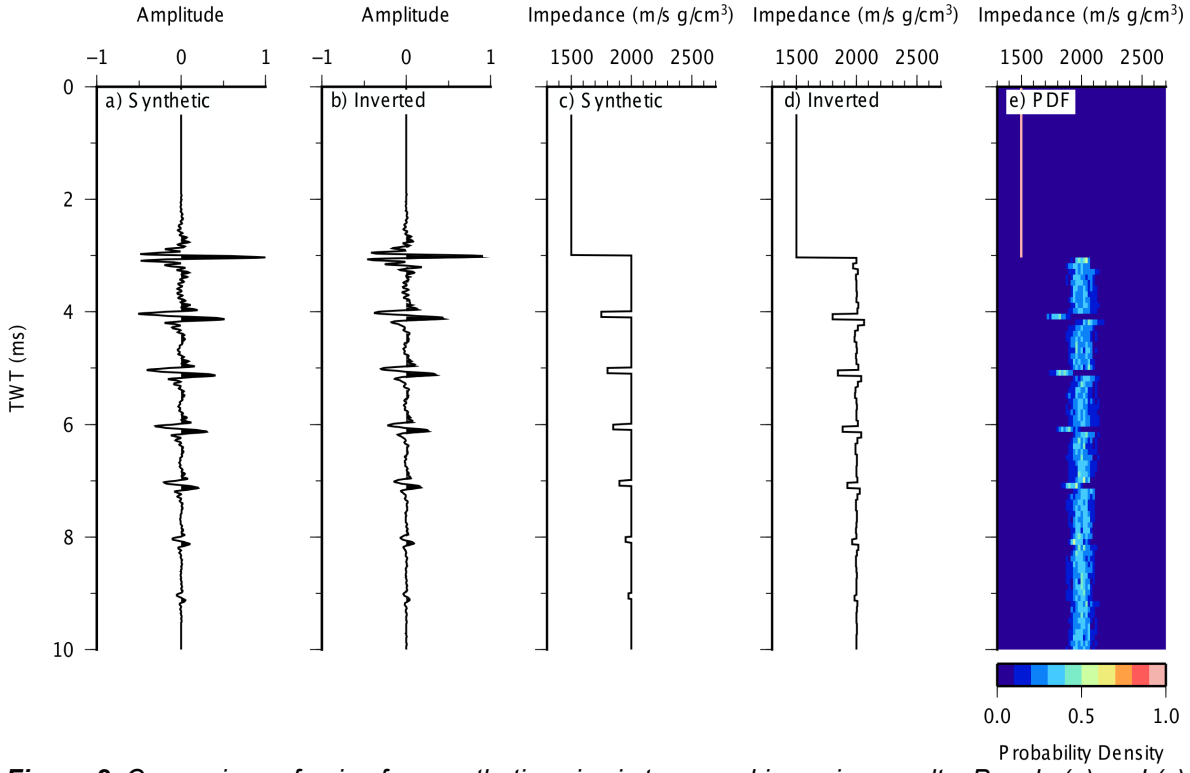

Figure 2. *Comparison of noise free synthetic seismic trace and inversion results. Panels (a) and (c) show the synthetic trace and accompanying impedance profile, respectively, while panels (b) and (d) show the associated inversion results. Panel (e) presents the Probability Density Function for the inverted impedance model derived from 200 independent runs.*

3 SYNTHETIC EXAMPLE

To illustrate the application of a GA for the inversion of high-resolution marine seismic reflection data, we first invert a noise-free synthetic example (Fig. 2). The synthetic trace was generated using a Chirp source wavelet that sweeps linearly from 1.5 kHz to 13.0 kHz over 32 ms with sine-squared to the 8th power tapers[14]. The synthetic earth model consisted of; a strong seafloor interface with an impedance contrast of +500 m/s g/cm^3, above a sequence of stacked, low impedance thin beds 1.0 ms TWT apart and 0.1 ms TWT thick. The impedance contrast between the thin beds and the background impedance systematically reduced with depth, consisting of: -250 m/s g/cm^3 at 1.0 ms TWT below the seafloor; -200 m/s g/cm^3; -150 m/s g/cm^3; -100 m/s g/cm^3; -50 m/s g/cm^3; and -25 m/s g/cm^3 at 6.0 ms TWT below the seafloor. This resulted in subsurface reflection amplitudes varying between half and 1/20th of the seafloor reflection amplitude.

The thickness of the thin beds was deliberately chosen such that it should theoretically be resolvable given a source waveform of the frequency bandwidth used, but still challenged the ability of the inversion algorithm to constrain high-fidelity sub-surface structure where reflected wavelets interact. The reducing impedance contrast between the thin beds and background simultaneously provided an insight into the limiting impedance contrast resolution of the algorithm.

3.1 Confidence Limits

Figure 2 shows the results of running a post-stack acoustic impedance inversion of the noise-free synthetic data example. Figure 2a and 2b compare the original and inverted trace data, whereas Figures 2c and 2d compare the original and inverted impedance structure. The inversion results presented in Figures 2b and 2d were generated from 200 independent inversions, each with 500 generations consisting of 900 models and with cross-over and mutation probabilities of 0.5 and

0.001, respectively. Figure 2d corresponds to the median impedance value calculated at each subsurface sample from the final model outputs for all 200 independent runs, and therefore represents the statistically 'best' impedance estimate for each subsurface sample. Figure 2b is the synthetic trace generated from this 'best' impedance model.

The inverted 'best' impedance model and trace very closely match the synthetic data. Both the amplitude and phase of the seismic trace are excellently replicated, while the thickness and amplitude of the thin beds are well replicated in the inverted impedance data. There is some leakage of structure around the thin beds resulting in small increases in impedance (up to 30 m/s g/cm^3) immediately above and below each bed, which is indicative of the inversion slightly over complicating the impedance profile in an attempt to replicate the complex composite wavelets formed by these thin beds (a common issue with similar inverse problems).

In addition to deriving a 'best' impedance model, the GA also permits the calculation of statistically robust PDFs for each subsurface sample, shown in Figure 2e where warmer colours correspond to impedances with a higher probability density. These results indicate that for most samples the absolute 95 % confidence limits associated with the value of the 'best' impedance model are ≤ ± 50 m/s g/cm^3. However, these results also indicate that the sensitivity to relative changes in acoustic impedance between adjacent samples is better than 50 m/s g/cm^3, with all thin beds down to the -50 m/s g/cm^3 bed at 8.0 ms TWT demonstrating both a well defined structure in the 'best' impedance model (Fig. 2d) and a clear deviation in the PDF (Fig. 2e). These results also indicate that, although the deepest thin bed (-25 m/s g/cm^3 at 9.0 ms TWT) is replicated in terms of trace structure and a small deviation in the 'best' impedance model, this structure falls within the 95 % confidence limits and therefore would be considered statistically questionable. An interpreter could therefore only be confident in the legitimacy of this low impedance structure were it to be replicated across multiple adjacent traces.

3.2 Noise Contamination

The contamination of high-resolution marine seismic reflection data with significant noise levels is a common problem. The shallow tow depths (typically < 1.0 m) and short layback distances behind the vessel (typically 20 – 50 m) combine with the small source sizes (typically c. 215 dB re 1 uPa at 1 m for Chirp and Boomer sources) to simultaneously increase the background noise level and decrease the signal. In contrast, traditional reservoir-scale marine seismic reflection surveys use tow depths of 3 – 10 m, laybacks ranging from 100s m to several km, and source arrays with a combined power level commonly in excess of 250 dB re 1 uPa at 1 m (an increase in power ratio of over four orders of magnitude). Additionally, reservoir-scale marine seismic acquisition often involves a large towed array of several hundred receivers, affording effective noise cancellation through stacking that is not possible for most shallow-water applications, where commonly only a single hydrophone or short streamer are deployed. This makes the application of inversion to high-resolution marine seismic reflection data a highly non-unique problem, resulting in an inversion space that can be characterized by multiple local minima. A suitable inversion algorithm must therefore be effective at finding a sensible approximation of the global solution.

To investigate the robustness of the GA inversion algorithm in the presence of noise, the synthetic trace data presented in Figure 2 were contaminated with random noise at a range of S/N levels. Figure 3 presents the results of running the inversion using the same parameterization as for the noise-free case, but using traces contaminated with S/N ratios of 20, 10, and 5 with respect to the seafloor reflection amplitude (i.e., much worse S/N ratios with respect to the reflections from the thin beds). In terms of impedance contrasts, these S/N values conform to noise on the impedance profile of up to ± 25 m/s g/cm^3, ± 50 m/s g/cm^3, and ± 100 m/s g/cm^3, respectively. Figure 3a shows the noise-free impedance profile used to generate the synthetic traces, while Figures 3b through 3d show the inverted impedance profiles in the S/N = 20, 10, and 5 cases, respectively. Black lines indicate 'best' impedance model, while shaded grey region 95 % confidence limit. Figure 3e shows the noise-free trace together with the noise-contaminated traces used as input to the inversions.

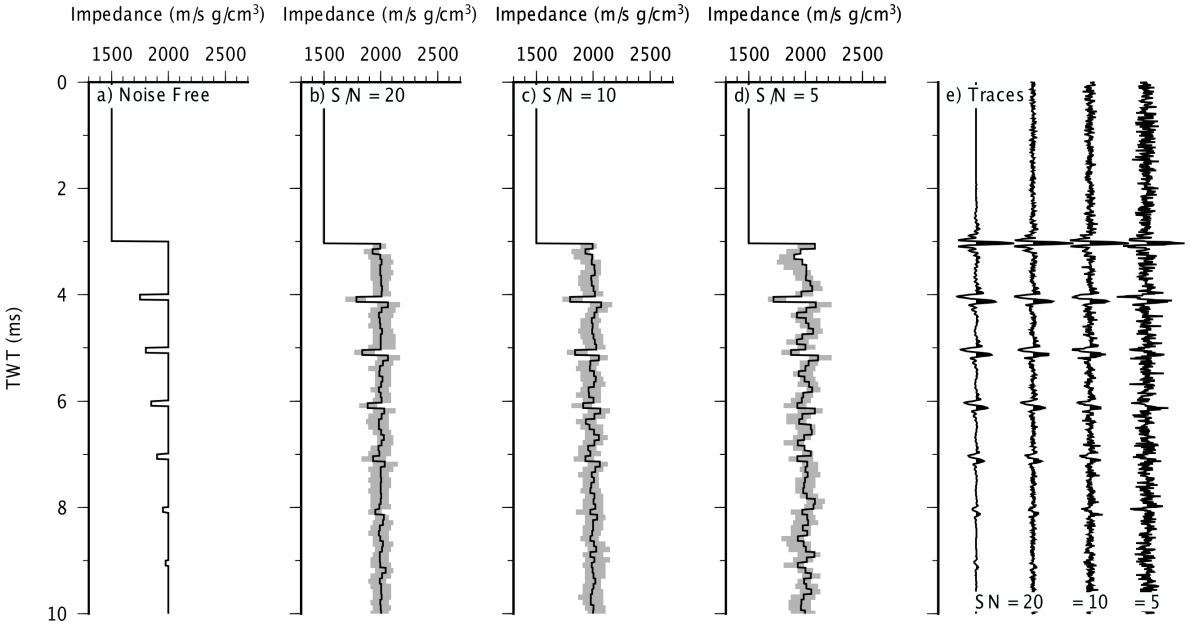

Figure 3. *Inversion results using synthetic trace data contaminated with random noise. Noise-free impedance structure is shown in panel (a), while inverted impedance structure for S/N = 20, 10, and 5 cases are shown in panels (b) through (d). Panel (e) shows traces used for inversion.*

For the S/N = 20 case (Fig. 3b), the noise level of ± 25 m/s g/cm^3 is approaching the amplitude of the -50 m/s g/cm^3 thin bed at 8 ms TWT. However, this impedance thin bed is still reconstructed in both the 'best' impedance model and the 95 % confidence limits. For the S/N = 10 case (Fig. 3c), the top 3 thin beds are accurately reconstructed, while the 4th thin bed (-100 m/s g/cm^3), although replicated in amplitude, is less well constrained in thickness due to a discrete, high amplitude noise spike c. 0.2 ms TWT above the bed reflection (Fig. 3e). For the S/N = 5 case (Fig. 3d), only the shallowest thin bed is accurately reproduced, while the thickness of the second is over estimated and the wavelet for the third is significantly altered by noise, resulting in the inversion reconstructing a positive impedance contrast thin bed.

These results demonstrate that the GA is effective at deriving a sensible approximation of the global minimum, even in the presence of relatively high levels of noise. In all cases where the reflected wavelet from each thin bed is reasonably representative of the noise-free case, the inversion accurate reproduces both the amplitude and thickness of the original bed. Only when that wavelet becomes significantly altered from it's original amplitude and/or phase does the inversion fail to reproduce the noise-free thin bed structure, which is to be expected given that the inversion result is derived solely from the trace data. It should also be noted that the S/N = 5 is an extreme case and would present a difficult prospect for traditional qualitative stratigraphic interpretation.

4 REAL DATA EXAMPLES

Inverting the synthetic data example presented in Figures 2 and 3 demonstrates, in principle, that a GA can be used to reliably derive subsurface acoustic impedance information and confident limits from high-resolution marine seismic reflection data under a variety of noise conditions. To illustrate that this method can be applied in practice to real, field data (which may include both random and systematic noise as well as other acquisition irregularities), a case study data set acquired in the Sørfjorden side-fjord of Northern Norway[15,16,17] is presented. These data include a decimeter-resolution 3D Chirp seismic volume, short-streamer 2D Boomer and Sparker multi-channel seismic reflection profiles, two 15-m long piston cores and multiple pushed and free-fall cone penetrometer profiles[16]. Of particular interest at this site is a 40 cm thick, clay-rich thin bed c. 3.5 m below the seafloor that contains the glide plane for multiple shallow landslides[15,17].

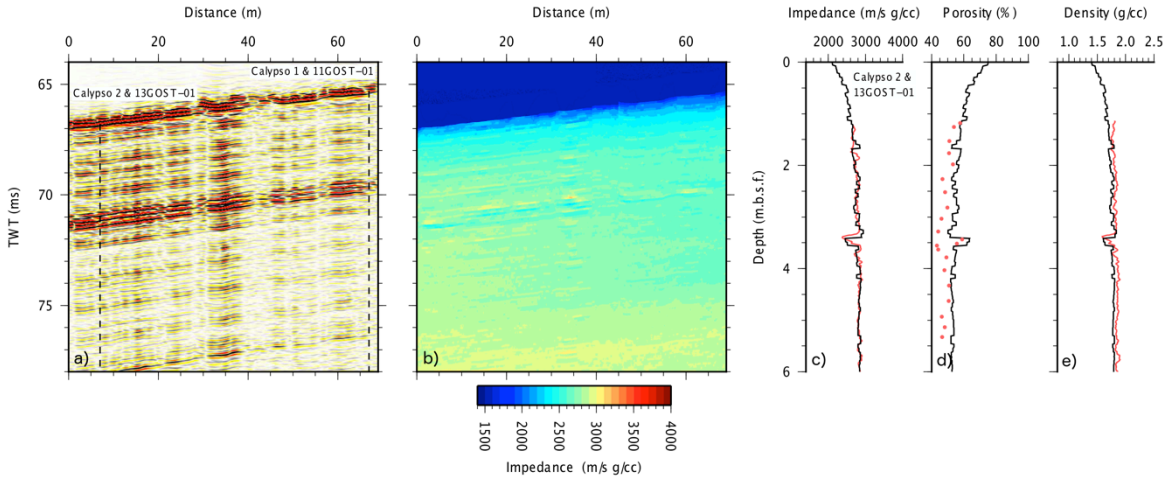

Figure 4. *Inversion applied to Chirp sub-bottom profiler data. Panel (a) shows Chirp profile, panel (b) the inverted impedance profile, and panels (c) through (e) compare derived properties with direct samples for coincident core location.*

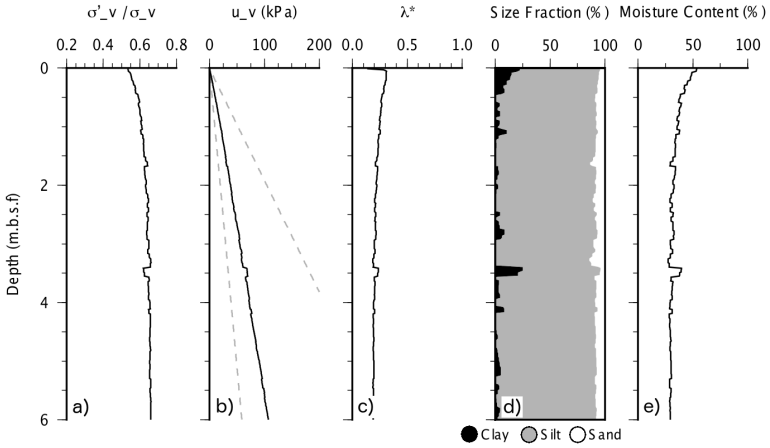

Figure 5. *More detailed soil mechanical properties derived from the inversion results after conversion into the depth domain, including: stress ratio; pore pressure; over pressure ratio; clay/silt/sand size fraction; and moisture content.*

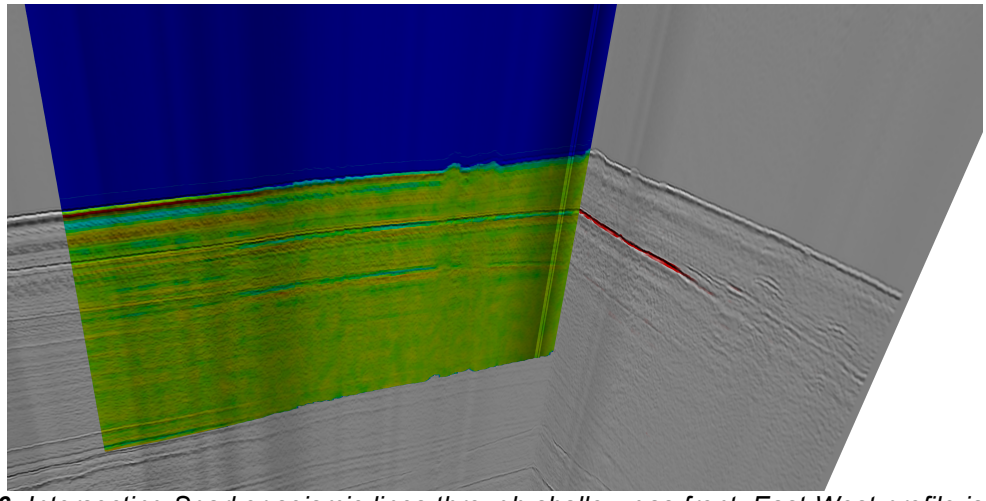

Figure 6. *Intersecting Sparker seismic lines through shallow gas front. East-West profile is overlain by inverted acoustic impedance profile, highlighting gas front as low impedance anomaly. North-South profile is overlain by gas saturations calculated using Wood's equation.*

Figure 4 presents the results from performing the inversion on an arbitrary profile extracted from the 3D Chirp volume that intersects the two core locations. Figure 4a shows the Chirp profile used for the inversion, Figure 4b the acoustic impedance profile produced by the inversion. From these impedance data a number of basic soil properties (including P-wave velocity, density, and porosity) can be calculated using empirical relationships derived from published data[8].

Deriving such soil properties using inversion techniques permits these properties to be mapped spatially, no longer being constrained to 1D core or borehole localities. Furthermore, deriving a high-resolution P-wave velocity model permits the inverted data to be converted from TWT into depth below the seafloor. This permits the derived soil properties to be plotted in the domain that is most useful to engineers, as well as allowing for more robust comparison with direct sampled data. Figures 4c through 4e compares the inverted impedance, porosity and density (solid black lines) with coincident data derived from the piston core Calypso 2 (red). The impedance and density data were measured on the split core using a Multi-Sensor Core Logger (MSCL), while the porosity was calculated from water content measurements. The inversion results demonstrate an excellent agreement with the direct sampled data, accurately reproducing the observed structure and replicating the thickness and magnitude of the impedance, porosity, or density contrast associated with the clay-rich thin bed.

Additionally, the translation of these properties into the depth domain permits the calculation of more detailed soil mechanical properties. Integration of the bulk density profile with depth times gravity allows the vertical component of the effective stress (σ'_v) to be calculated, while a similar integration of the grain density (derived from the bulk density using porosity) allows the vertical component of the total stress (σ_v) to be calculated[18]. Assuming the vertical stress gradient dominates over the lateral stress gradient, the difference between the effective and total stresses is the pore pressure and therefore permits an estimate of the *in situ* pore pressure (u_v) and over pressure ratio (λ^*) to be calculated and spatial variability mapped using the seismic reflection data (Figures 5a through 5c). Furthermore, where there is clear evidence for a gas front in the Sørfjorden study area[7,17], it is possible to estimate gas saturation using an appropriate rock physics model. Assuming small gas bubbles and low gas saturation (reasonable given the environment), then the gas saturation can be estimated using a simplified version of Wood's equation[19]:

$$\beta = \frac{2\kappa P_0}{v_{sed}^2 \rho_{sed}} \left(1 - \frac{v_{eff}}{v_{sed}}\right) \quad (4)$$

where β is the gas saturation, κ the polytropic index, P_0 the hydrostatic pressure, v_{sed} and ρ_{sed} the velocity and density of the background sediment, and v_{eff} the velocity of the sediments containing gas bubbles.

Using a polytropic index appropriate for biogenic gas (1.3[20]) the gas saturation was estimated as between 0.05% and 0.20%, in agreement with previously published results[7]. Figure 6 shows intersecting impedance and gas saturation profiles from Sørfjorden.

5 CONCLUSIONS

The work presented demonstrates the potential for deriving a range of *in situ* soil properties for the shallow sub-surface using post-stack acoustic impedance inversion applied to high-resolution marine seismic reflection data. The synthetic results suggest that the combination of a GA for optimization and a convolutional forward model is a robust inversion solution in the presence of moderate noise levels (providing a sensible approximation of the global minimum even when noise amplitudes were approaching signal amplitudes), and provides additional assurance on the statistically 'best' impedance model through the generation of associated 95% confidence limits. Additionally, we have shown that, through the use of empirical relationships to relate acoustic impedance with basic sediment properties (P-wave velocity, density, and porosity), it is possible to derive estimates of more complex soil mechanical properties and therefore provides a first step towards remote geotechnical characterization of the marine shallow section.

6 REFERENCES

1. J. Morgan, M. Warner, R. Bell, J. Ashley, D. Barnes, R. Little, K. Roele and C. Jones, Next-generation seismic experiments: wide-angle, multi-azimuth, three-dimensional, full-waveform inversion, Geophysical Journal International 195(3), 1657–1678 (2013).
2. S. Operto, Y. Gholami, V. Prieux, A. Ribodetti, R. Brossier, L. Metivier, and J. Virieux, A guided tour of multiparameter full-waveform inversion with multicomponent data: From theory to practice, The Leading Edge, 32(9), 1040-1054 (2013).
3. C. Wagner, A. Gonzalez, V. Agarwal, A. Koesoemadinata, D. Ng, S. Trares, N. Biles and K. Fisher, Quantitative application of poststack acoustic impedance inversion to subsalt reservoir development, The Leading Edge 31(5), 528–537 (2012).
4. X.-Q. Ma, Simultaneous inversion of prestack seismic data for rock properties using simulated annealing, Geophysics, 67(6), 1877-1885 (2002).
5. S. Panda, L.R. LeBlanc and S.G. Schock, Sediment classification based on impedance and attenuation estimation, J. Acoust. Soc. Am., 96(5), 3022-3035 (1994).
6. L.J.W. Pinson, T.J. Henstock, J.K. Dix and J.M. Bull, Estimating quality factor and mean grain size of sediment from high-resolution marine seismic data, Geophysics, 73(4), G19-G28 (2008).
7. E.C. Morgan, M. Vanneste, I. Lecomte, L.G. Baise, O. Longva and B. McAdoo, Estimation of free gas saturation from seismic reflection surveys by the genetic algorithm inversion of a P-wave attenuation model, Geophysics, 77(4), R175-R187 (2012).
8. M.E. Vardy, Deriving shallow sediment properties using post-stack acoustic impedance inversion, Near Surface Geophysics, 13(2), 143-154 (2015).
9. R. Sheriff, Encyclopedic Dictionary of Applied Geophysics. In: Geophysical Reference Series 13, SEG, 4th Edition (2002).
10. D. Goldberg, Genetic Algorithms in Search, Optimization, and Machine Learning, Addison Wesley Publishing Company, Reading, MA (1989).
11. P. Stoffa and M. Sen, Nonlinear multiparameter optimization using genetic algorithms: inversion of plane wave seismograms, Geophysics, 56(11), 1794–1810 (1991).
12. R. Sivaraj and T. Ravichandran, A review of selection methods in Genetic Algorithms, International Journal of Engineering Science and Technology, 3(5), 3792–3797 (2011).
13. S. Kirkpatrick, C. D. Gelatt and M. P. Vecchi, Optimization by Simulated Annealing, Science, 220(4598), 671–680 (1983).
14. M. Gutowski, J. Bull, T. Henstock, J. Dix, P. Hogath, T. Leighton and P. White, Chirp sub-bottom profiler source signature design and field testing, Marine Geophysical Researches, 23, 481-492 (2002).
15. J.-S. L'Heureux, O. Longva, A. Steiner, L. Hansen, M. Vardy, M. Vanneste et al., Identification of Weak Layers and Their Role for the Stability of Slopes at Finneidfjord, Northern Norway. In: Submarine Mass Movements and Their Consequences 31, Advances in Natural and Technological Hazards Research, pp. 321–330, Springer, Heidelberg, DE (2012).
16. M. Vanneste, J.-S. L'Heureux, J. Brendryen, N. Baeten, J. Larberg, M. Vardy et al., Assessing offshore geohazards: A multi-disci- plinary research initiative to understand shallow landslides and their dynamics in coastal and deepwater environments, Norway. In: Submarine Mass Movements and Their Consequences, vol. 31 of Advances in Natural and Technological Hazards Research, pp. 29–41, Springer, Heidelberg, DE (2012).
17. M. Vardy, J.-S. L'Heureux, M. Vanneste, O. Longva, A. Steiner, C. Forsberg et al., Multidisciplinary investigation of a shallow near-shore landslide, Finneidfjord, Norway, Near Surface Geophysics 10, 267–277 (2012).
18. R.F. Craig, Craig's Soil Mechanics, Taylor and Francis, Oxford, UK, 7th Edition (2004).
19. T. Leighton and G. Robb, Preliminary mapping of void fractions and sound speeds in gassy marine sediments from subbottom profiles, JASA Express Letters, 124(5), EL313 – EL320 (2008).
20. T. Leighton, S. Meers and P. White, Propagation through nonlinear time-dependent bubble clouds and the estimation of bubble populations from measured acoustic characteristics, Proc. R. Soc. London Ser. A, 460, 2521–2550 (2004).